Human Temporomandibular Joint Motion: A Synthesis Approach for Designing a Six-Bar Kinematic Simulator

Michel Demuynck
Department of Mechanical Engineering,
École de technologie supérieure,
Université du Québec,
Montréal, QC H3C 1K3, Canada
e-mail: michel.demuynck.1@ens.etsmtl.ca

Aidin Delnavaz
Department of Mechanical Engineering,
École de technologie supérieure,
Université du Québec,
Montréal, QC H3C 1K3, Canada
e-mail: aidin.delnavaz@ens.etsmtl.ca

Jérémie Voix
Department of Mechanical Engineering,
École de technologie supérieure,
Université du Québec,
Montréal, QC H3C 1K3, Canada
e-mail: jeremie.voix@etsmtl.ca

The human earcanal can accommodate several types of in-ear devices including hearing aids, earphones, hearing protectors, and earplugs. This canal-type home has a neighbor called the temporomandibular joint (TMJ) whose movements slightly deform the shape of the earcanal. While these cyclic deformations can influence the positioning, comfort, and functioning of ear-fitted devices, they can also provide a significant amount of energy to harvest. Given their importance, the TMJ movements and earcanal deformations have been well studied. However, their mutual actions are still not fully understood. This paper presents the development of a six-bar kinematic TMJ simulator capable of replicating the complicated motion of the jaw. The development relies on a two-phase mechanism design algorithm to numerically optimize and analytically synthesize linkage mechanisms for which the classical optimization approaches cannot return a converged solution. The proposed algorithm enables the design of a kinematic simulator to generate the TMJ path with an average error as low as 1.65% while respecting all the hinge-axis parameters of the jaw. This algorithm can be subsequently used to solve nonlinear complex linkage synthesis problems, and ultimately, the developed kinematic simulator can be used to further investigate TMJ–earcanal interactions.
[DOI: 10.1115/1.4050828]

Keywords: bio-inspired design, mechanism design, mechanism synthesis, theoretical kinematics

1 Introduction

The human body is able to move, thanks to the joints that connect its bones. One of the body's most interesting joints is located in the area of the head, the temporomandibular joint (TMJ). Also called the jaw joint, it is involved in many activities including eating, speaking, chewing, laughing, etc. More specifically, the TMJ is the bony protuberance of the jaw called the mandibular condyle hosted within the fossa of the temporal bone of the skull. Many studies show the mechanical influence the TMJ exerts on its surrounding soft tissues when the jaw opens and closes. This movement results in geometrical deformations of the earcanal, also called earcanal dynamic movement [1]. The earcanal movements caused by TMJ activity possess some kinetic energy, which can be harvested to power the electronic circuits of in-ear devices. Energy harvesting from within the earcanal has been studied in recent years and a few energy scavenger prototypes have been developed. However, the exact magnitude of the earcanal deformations and the amount of energy available from TMJ activity are yet to be investigated. Given the small size and curving shape of the earcanal, the TMJ is hard to access for in vivo measurements. Furthermore, the biomechanical interactions between the TMJ and the earcanal are not yet fully understood. So far, two methods have been proposed to quantify the earcanal dynamic movement: (1) an experimental method consisting of a hydraulic system that transforms the earcanal deformation into a measurable pressure variation in a water column [1,2] and (2) an analytical method based on the bending beam theory to model the earcanal wall deformation [3]. Although the results are encouraging, the extent to which the modeling used was simplified throws into question the accuracy of the results, thus calling for a more precise modeling of the TMJ–earcanal interactivity and interactions.

Up to now, TMJ activity and the earcanal's shapes and deformations have been separately investigated by many groups of researchers. The complex kinematic of the TMJ has been studied either in 2D or 3D, by focusing either on the incisor path [4–7] or the mandibular condyle path [8–11] or the mandibular helical axis path [12,13]. These studies provide more insight into the mechanical behavior of the TMJ in different ranges of motion including elevation/dropping, lateral deviation, and protraction/retraction of the jaw. The forces applied by the TMJ during mastication have also been the topic of many experimental studies. Some types of jaw motion simulators, replicators, or robots have been developed to measure the TMJ loads during mastication. All these robotic platforms mimic both the kinematics and dynamics of the jaw movement either in a simple one degree-of-freedom (1-DOF) model [14] or a 3-DOF model [15–17] or more recently in a complicated 6-DOF model [18,19]. In addition, the dental articulators which are currently in use by dentists and orthodontists enable the reproduction of some or all of the movements of the mandible (lower jaw) in relation to the maxilla (upper jaw) to assist in the accurate fabrication of prosthodontic or orthodontic appliances.

On the other hand, the earcanal geometry and its associated dynamic movements have been the subject of many studies by audiologists and hearing conservationists to improve the process of ear impression required to make customized hearing aids and custom-fitted earplugs [20–22]. To the best of the authors' knowledge, a comprehensive study involving both TMJ and earcanal as well as their mutual interactions is still lacking in the literature. To this end, a TMJ–earcanal simulator based on a planar linkage mechanism is required to investigate how the TMJ deforms the earcanal and how the earcanal reacts to the TMJ forces during jaw joint activity.

One of the best candidates to achieve an optimal TMJ–earcanal simulator is a planar linkage mechanism. Planar linkage assemblies are widely used to design anatomic prostheses, humanoid robots, or exoskeletons capable of mimicking the human body's joint motions. Compared to servo-controlled devices such as machine tool arms, the proposed linkage mechanism control design has the clear advantage of being much less expansive and much simpler to duplicate as a research tool: the integration of the proposed mechanics with an electrical motor could reproduce the TMJ's anatomical behavior with a rotational input movement. Compared to other motion-transforming mechanisms such as cam-and-roller or rack-and-pinion, linkage mechanisms are capable of offering more complex types of motion while requiring a simpler architecture and fewer joints. Also, the theory of such mechanisms is well known which makes their synthesis, design, and analysis

Contributed by the Mechanisms and Robotics Committee of ASME for publication in the Journal of Mechanisms and Robotics. Manuscript received November 4, 2020; final manuscript received March 29, 2021; published online June 1, 2021. Assoc. Editor: Gim Song Soh.

much easier to implement using an inverse dynamics solution. Path generation and motion generation are two important types of problems to be considered in the mechanism's synthesis. Path generation is the control of the mechanism coupler point passing through a desired set of discrete points while motion generation is the control of a coupler as a solid body in both position and orientation moving through a set of prescribed positions. Given the very limited number of design parameters for the linkage mechanisms, an optimization process is normally required for the mechanism synthesis.

Optimal synthesis of mechanisms can be found in many types of biomedical prosthesis design. For example, a cross four-bar linkage mechanism (FBLM) reproducing the movement of the middle finger of the human hand was presented in Ref. [23]. This type of mechanism is optimized according to the bending angle of the second phalanx by minimizing the mean quadratic error between the generated and desired values. An optimized *Stephenson* six-bar linkage mechanism (SBLM) capable of reproducing the trajectory of the ankle joint according to the hip joint for a human, walking exoskeleton was developed in Ref. [24]. The study proposed an 11-point path synthesis combined with an optimization process allowing the mechanism to pass through 60 accuracy points by minimizing the difference between the coupler point and the data points collected by a motion-capture sensor. Another kind of SBLM design was proposed for a three-jointed finger mechanism [25]. The position of the coupler and its orientation compared with the data of the distal segment of the human finger are minimized with the least squares criteria.

The purpose of this study is to propose a two-phase motion generation synthesis with a biomechanics-driven approach to design a SBLM reproducing the TMJ movement and replicating the jaw rotation during the mouth-opening motion. This paper will also evaluate the feasibility of designing a simplified-architecture mechanism that is only driven by revolute joints. The results of this paper could be useful to several fields including, but not limited to, the design of dental articulators, surgical mandibular implants, or devices used to cure TMJ disorders. Also, other studies relating to the interaction of the TMJ and earcanal such as those focused on earplug comfort [26], the hearing aid retention problem [27,28], or energy harvesting from earcanal dynamic movements [29–31] could substantially benefit from the results of this study.

2 Biomechanics of the Temporomandibular Joint

In order to study jaw joint movements and their influence on earcanal deformations, certain reference points describing the TMJ movements and constraints need to be defined. The hinge axis is defined as an imaginary line which is perpendicular to the mid-sagittal plane of the head, passing through the centers of both mandibular condyles as shown by point C in Fig. 1(*a*). In most studies, the hinge axis is a reference axis used to measure the kinematic parameters of the jaw movements such as the mandibular condyle path (yellow dashed line with both initial and final points C_1 and C_N), the incisor path $s_{incisor}$ (red line), and the sagittal rotation Φ_{hinge} (red arc) as illustrated in Fig. 1(*a*).

The geometrical path of the hinge axis represents the curvilinear translation of the mandibular condyle. The following mathematical function has been proposed by Peck et al. as a boundary condition for the mandibular condyle path when the jaw is opening [32], in which

$$y(x) = 5\cos\left(\frac{\pi}{13}x\right) - 5 \tag{1}$$

where x denotes the coordinate along the antero-posterior (A-P) axis and y denotes the coordinate along the supero-inferior (S-I) axis, both expressed in millimeters. In fact, this formula represents the shape of the temporal fossa of the skull bone, which is the superior anatomical bound of the mandibular condyle movement. As shown in Fig. 1(*a*), the orientation of the proposed profile follows the anatomical planes of the human head by a 40 deg rotation with respect to the occlusal plane and a 20 deg rotation with respect to the mid-sagittal plane. Moreover, the profile length corresponds to a 16 mm horizontal translation of the mandibular condyle along the A-P axis.

The hinge axis is also the axis around which the jaw performs its rotation when the mouth opens. This rotation induces a curvilinear translation of the incisor. Several studies have focused on the relationship between the incisor and the condylar paths. For example, a 32.05 ± 0.90 deg sagittal rotation of the jaw can be associated to a 48.60 ± 1.03 mm curvilinear translation of the incisor by tracking the jaw using an optoelectric device [4].

For this preliminary study, the following parameters are assumed: the occlusal plane is horizontal, the hinge-axis opening rotation of the jaw Φ_{hinge} is fixed at a clockwise rotation of 32 deg, and the mouth-opening movement is symmetrical between the left and right TMJ. The *target path* is defined as a set of discrete positions resulting from the function presented in Eq. (1) after performing the anatomical transformations (40 deg orientation according to the occlusal plane and 16 mm truncation of the translation path). Since the study frame is based on the parasagittal plane passing

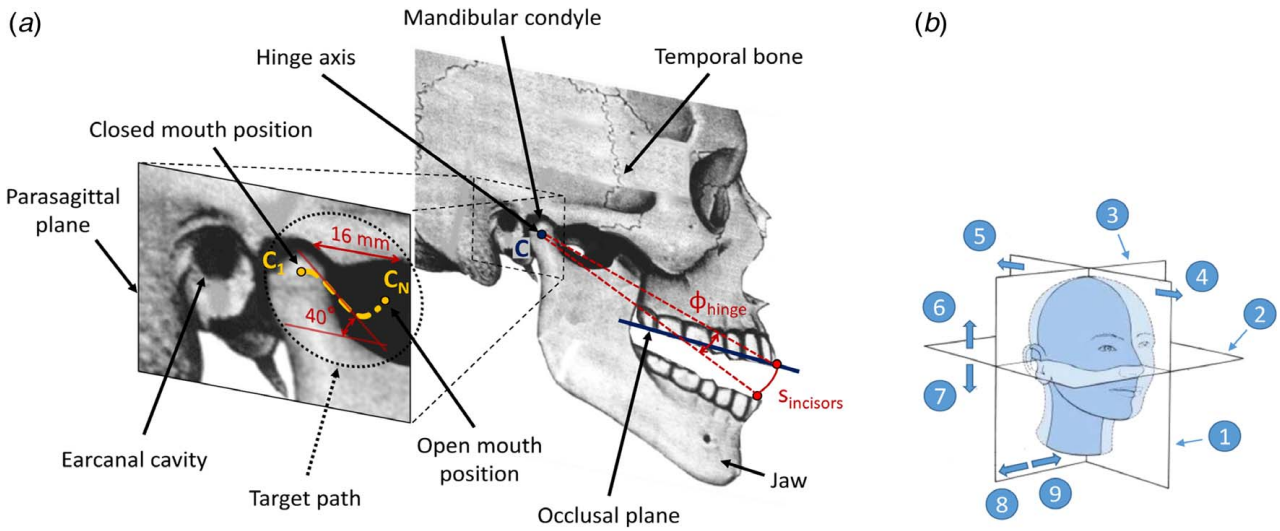

Fig. 1 (*a*) Anatomical setting of the TMJ model and (*b*) anatomical planes and axes associated with the head: (1) median or mid-sagittal plane, (2) horizontal or transverse plane, (3) frontal or coronal plane, (4) anterior axis, (5) posterior axis, (6) superior axis, (7) inferior axis, (8) lateral axis, and (9) medial axis

through the mandibular condyle center, the angular orientation of the temporal fossa profile according to the mid-sagittal plane will not be considered. The mandibular condyle is assumed as going back-and-forth along the profile described by the anatomical-adjusted function of Peck et al. The curvilinear length of the incisor path s_{incisor} is assumed to be 50 mm.

3 One-Phase Optimization Approach: Motion Generation Synthesis

Several mechanisms can be used to generate a continuous path passing through a set of specified discrete positions. The mechanism should be able (1) to perform a planar (2D) motion as the target path is a 2D curve, (2) to be driven by one input signal so as to have the simplest possible controls, and (3) to favor pivoted links over slider links as the design and implementation of pivoted links are technically much simpler than those of slider links. Based on these criteria, the FBLM-1 composed only of pivoted or rotating joints is the best choice for this study. Figure 2 schematically shows the FBLM-1 model in its initial (solid line) and intermediate (dashed line) positions after an arbitrary rotation of $\Delta\theta_A$ for the input link.

As illustrated in Fig. 2, 11 design variables can be identified for the FBLM-1 model: the lengths of all the links l_1, l_2, l_3, l_4, and l_C, the global orientation of the mechanism according to its angle α with respect to the reference A-P axis, the coupler angle γ, the initial angular position of the input link $\theta_{A,0}$, the angular variation of the input angle $\Delta\theta_A$, and the coordinates $[x_A,y_A]$ of point A. The global (x, y) and local (u, v) frames are orthogonal coordinate systems fixed in point A, whose first axes are aligned with the reference A-P axis and link l_1, respectively, as shown in Fig. 2.

The optimized configuration of the FBLM-1 model should generate a path at point C that matches the target path as closely as possible, however the timing at which the point C reaches the precision points on the target path in terms of the input rocker angle is not of concern. To this end, the coordinates of the coupler point C should be expressed as a function of the design variables in the global coordinate system by

$$\begin{cases} x_C = x_A + l_2\cos(\theta_A + \alpha) + l_C\cos(\gamma + \theta_P + \alpha) \\ y_C = y_A + l_2\sin(\theta_A + \alpha) + l_C\cos(\gamma + \theta_P + \alpha) \end{cases} \tag{2}$$

It is therefore necessary to express the design parameter θ_P as a function of the design variables using Freudenstein's method [33]. Projecting the geometric loop in Fig. 2 onto the directions $\vec{u}$ and $\vec{v}$ yields:

$$\begin{cases} l_2\cos(\theta_A) + l_3\cos(\theta_P) - l_4\cos(\theta_B) - l_1 = 0 \\ l_2\sin(\theta_A) + l_3\sin(\theta_P) - l_4\sin(\theta_B) = 0 \end{cases} \tag{3}$$

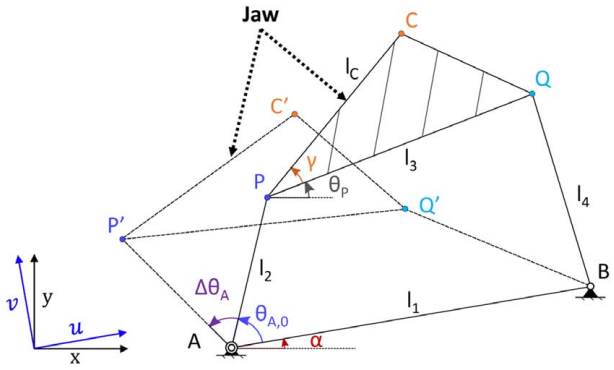

Fig. 2 Schematic representation of the FBLM-1 in its initial (solid line) and intermediate (dashed lines) positions

By eliminating θ_B in Eq. (3) and using $K_1 = l_1/l_2$, $K_2 = l_1/l_4$, and $K_3 = l_4^2 - l_1^2 - l_2^2 - l_3^2/2l_2l_3$, one can obtain

$$K_1\cos(\theta_P) + K_2\cos(\theta_A) + K_3 = \cos(\theta_P)\cos(\theta_A) + \cos(\theta_P)\cos(\theta_A) \tag{4}$$

Then, using the half-angle entities in Eq. (4), a quadratic polynomial of unknown $\tan(\theta_P/2)$ can be expressed as

$$A\tan^2\left(\frac{\theta_P}{2}\right) + B\tan\left(\frac{\theta_P}{2}\right) + C = 0 \tag{5}$$

in which

$$\begin{aligned} A &= (1 + K_2)\cos(\theta_A) - K_1 + K_3 \\ B &= -2\sin(\theta_A) \\ C &= K_1 + (K_2 - 1)\cos(\theta_A) + K_3 \end{aligned}$$

Finally, θ_P is derived by solving Eq. (5):

$$\theta_{P_{1,2}} = 2\arctan\left(\frac{-B \pm \sqrt{B^2 - 4AC}}{2A}\right) \tag{6}$$

Equation (6) potentially provides two solutions, each corresponding to a specific configuration of the mechanism: "+" represents the solution of the open configuration (none of the links are crossed), whereas "−" corresponds to the crossed configuration (two links cross over each other). The optimization process takes into account both configurations. By replacing Eq. (6) into Eq. (2), the coordinates of point C are expressed as a function of the design variables.

For the optimization process, the target path is modeled as an interpolation of $N = 50$ discrete precision points. Each of these points is compared to its associated generated point C_i, which corresponds to the angle value of $\theta_{A,i}$. The performance of the mechanism synthesis is evaluated based on the root-mean-square error (RMSE) between the target and the generated path, normalized to the arc length of the target path s_{target} in millimeters within the target zone. Therefore, the optimum design is obtained by minimizing the following objective function:

$$\epsilon = \frac{\sqrt{(1/N)\sum_{i=1}^{N}\left[(x_{\text{target},i} - x_{C,i})^2 + (y_{\text{target},i} - y_{C,i})^2\right]}}{s_{\text{target}}} \tag{7}$$

The optimized FBLM-1 model would be physically realizable and biomechanically capable of reproducing the movement of the jaw if the following constraints were satisfied:

Constraint #1: The size of the links should remain within an acceptable range in order to minimize the space requirement;

$$15\,\text{mm} \le l_i \le 150\,\text{mm} \quad \forall i \in \{1, 2, 3, 4\} \tag{8}$$

Constraint #2: The Grashof condition should be imposed to ensure the smooth movement of the mechanism in its operating range including the entire target curve:

$$\begin{aligned} &2\min(\{l_1, l_2, l_3, l_4\}) + 2\max(\{l_1, l_2, l_3, l_4\}) \\ &\quad - (l_1 + l_2 + l_3 + l_4) \le 0 \end{aligned} \tag{9}$$

Constraint #3: Link 2 is the input crank and should be capable of rotating a full 360 deg without any restriction or toggle position. Therefore, link 2 should be the shortest link in the mechanism whereby its length l_2 should be the shortest of all the links:

$$l_2 \le l_i \quad \forall i \in \{1, 3, 4\} \tag{10}$$

Constraint #4: The incisor movement is modeled by point P in Fig. 2 and so, the curvilinear path of point P should be equal to s_{incisor}:

$$l_2 \Delta\theta_A = s_{\text{incisor}} = 50\,\text{mm} \tag{11}$$

Constraint #5: The coupler should perform the biomechanical rotation Φ_{hinge} of the jaw:

$$\Delta\theta_P = \Phi_{\text{hinge}} = -32\,\text{deg} \tag{12}$$

The *fmincon* function with the sequential quadratic programing algorithm in the *Optimization Toolbox* of MATLAB (MathWorks, Natick, MA) is chosen as it is able to keep running the solving process of a nonlinear objective function even if the intermediate values are non-real. *fmincon* receives a number of input parameters including an initial set of the design variables. Therefore, it is necessary to run the optimization process using different initially guessed variables to enlarge the design space. The solving process of the one-phase optimization approach is summarized in Fig. 3.

In this study, ten iterations of the process are performed for each open- and crossed-configuration of the FBLM-1 model. Finally, the optimized model is chosen based on the lowest RMSE criterion. Among the 20 results, the lowest RMSE is $\epsilon = 3.12\%$ for the open configuration, for which the optimized set of design variables are detailed in Table 1. Figure 4 shows the optimized generated path (dashed line) compared to the target path (solid line).

Although the optimized generated path can follow the target curve, the difference between the two curves is quite considerable as seen in Fig. 4. The general shape of the generated path is not sufficiently curved and does not exhibit an inflection point. Therefore, the first-order optimality value which is a measure of how close the solution points are to optimal is relatively high, equaling 192.77. Also, the maximum constraint violation value equaling 27.68 confirms that some constraints are evaluating far from their acceptable boundaries during the optimization process. These parameters indicate that the FBLM-1 model is not performing well and is overconstrained. Therefore, it is necessary to either relax some of the constraints or modify the architecture of the mechanism to divide the constraints between several links. The two-phase hybrid optimization approach presented in the following section aims to improve the shortcomings of the FBLM-1 model by imposing the constraints on two different links.

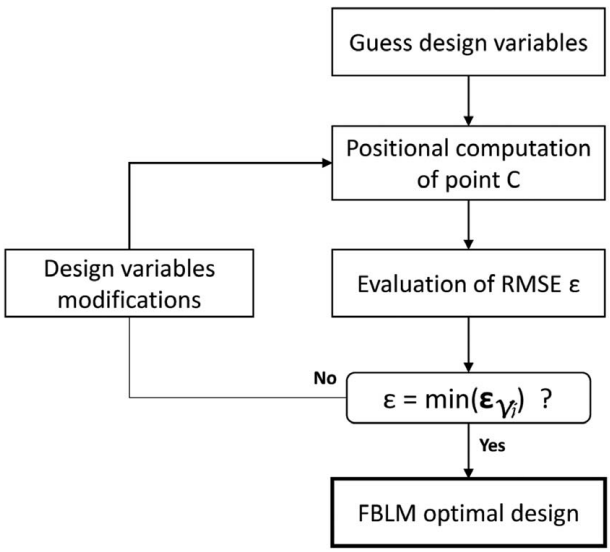

Fig. 3 Flowchart of the iterative process used to solve the one-phase optimization problem of the FBLM-1 model. ϵ_{V_i}, set of RMSE for the neighborhood of evaluation points at iteration "*i*".

Table 1 Optimized values of the design variables for the FBLM-1 model

l_1	123.45	mm
l_2	106.38	mm
l_3	150	mm
l_4	150	mm
l_C	143.72	mm
α	79.49 deg	
γ	0 deg	
$\theta_{A,O}$	206.36 deg	
$\Delta\theta_A$	25.31 deg	
x_A	69.61	mm
y_A	−1.06	mm

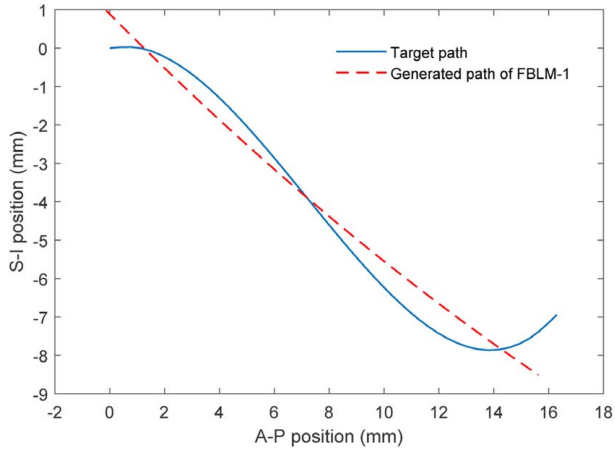

Fig. 4 Optimized generated path for the FBLM-1 model compared with the target path. Closed jaw position corresponds to the origin of the coordinate system.

4 Two-Phase Hybrid Optimization Approach: Path and Motion Generation Synthesis

The two-phase hybrid approach consists in synthesizing two separate linkages for the path and motion generation of the jaw and then integrating both subordinate mechanisms into the final setup. To this end, two different methods will be used to synthesize each sub-mechanism: (1) the numerical optimization approach is used for the path generation and (2) the analytical synthesis approach is adopted for the motion generation. Indeed, the proposed design is a marriage of a FBLM-2 to generate the desirable trajectory of point C and a three-rotational-joint (R) sub-mechanism called RRR-dyad to control the orientation of the jaw during its travel. The resulting mechanism is a SBLM, as illustrated in Fig. 5(*c*).

4.1 Path Generation Optimization of Four-Bar Linkage Mechanism-2. FBLM-2 is a four-bar closed mechanism composed of links l_1 through l_4 as shown in Fig. 5(*b*). Four out of the five constraints mentioned in the previous section are imposed to FBLM-2. In fact, constraint #1 to constraint #4 are all applied to FBLM-2, but constraint #5 is relaxed to make the generated path closer to the target path for point C. Except for the constraints, the optimization procedure for the FBLM-2 model remains quite similar to that of FBLM-1 with the same computational process, objective function, and optimization algorithm.

4.2 Analytical Motion Generation Synthesis of RRR-dyad. RRR-dyad is an open linkage consisting of links l_5 and l_6 as shown in Fig. 5(*a*). RRR-dyad is coupled to the FBLM-2 model via the joint located at C. This point represents the TMJ and l_6

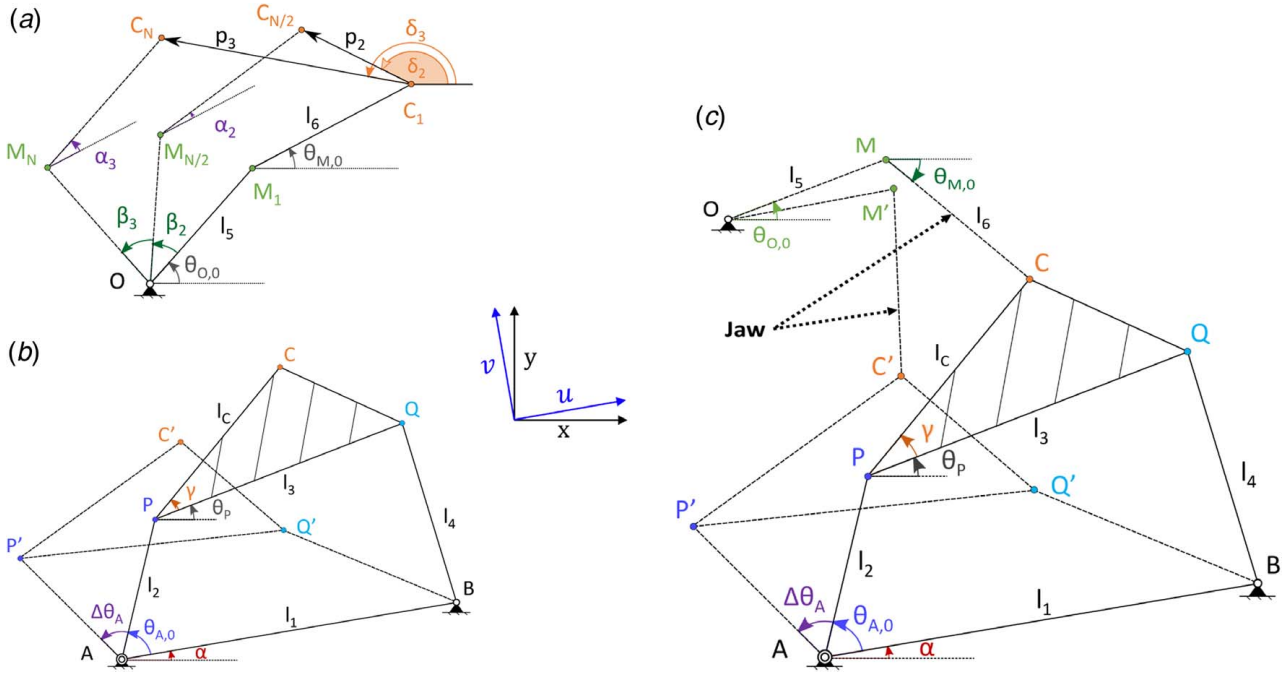

Fig. 5 Schematic representation of the (*a*) RRR-dyad model, (*b*) FBLM-2 model, and (c) SBLM model obtained by attaching (*a*) and (*b*) from point C. The initial positions are shown by the solid line.

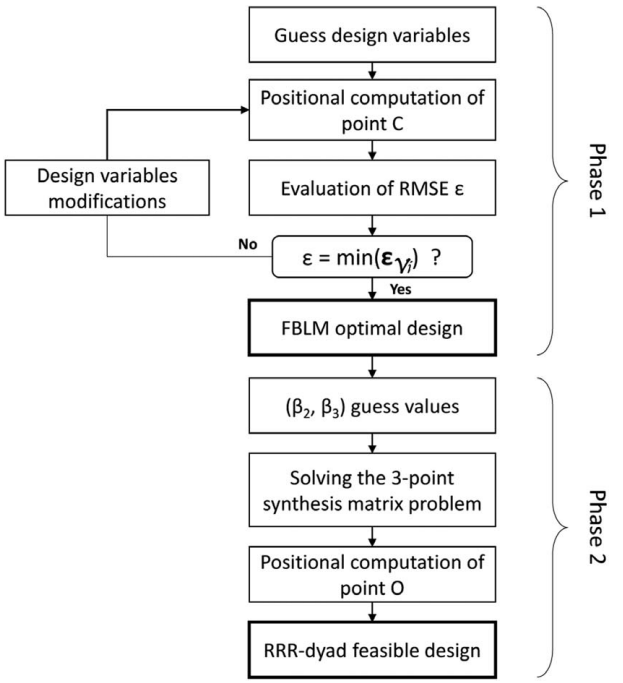

Fig. 6 Flowchart of the process for solving the two-phase hybrid optimization-analytical problem for the FBLM-2 and RRR-dyad models. ϵ_{V_i}, set of RMSE for the neighborhood of evaluation points at iteration "*i*."

Table 2 Optimized values of the design variables for the FBLM-2 model

l_1	137.72	mm
l_2	24.84	mm
l_3	26.94	mm
l_4	137.68	mm
l_C	34.47	mm
α	111.40 deg	
γ	14.04 deg	
$\theta_{A,O}$	185.16 deg	
$\Delta\theta_A$	108.42 deg	
x_A	17.53	mm
y_A	3.62	mm

Table 3 Values of the design variables for the analytical solution of the RRR-dyad model

l_5	17.06	mm
l_6	34.05	mm
$\theta_{O,0}$	6.64 deg	
$\theta_{M,0}$	113.19 deg	
x_O	−3.93	mm
y_O	−33.27	mm

represents the jaw. The RRR-dyad makes the jaw link l_6 pass through three specified positions of point C along the TMJ trajectory while controlling its orientation with the rotation angles α_2 and α_3 at the intermediate and final positions.

The analytical synthesis of the RRR-dyad for three precise positions is based on the algebraic analysis of the vector loops formed by its links in the starting, intermediate, and final positions. Therefore, three distinct positions of point C along the TMJ trajectory are chosen and the RRR-dyad model is schematically built at these positions as demonstrated in Fig. 5(*a*).

The design variables including l_5 and l_6, their initial angular positions, $\theta_{O,0}$ and $\theta_{M,0}$, their intermediate and final rotations α_2, α_3, β_2 and β_3 with respect to their initial angular positions, and the magnitude and orientation of the displacement vectors p_2, p_3, δ_2, and δ_3 to reach the intermediate and final positions can be identified in the model. Two vector loops are formed in Fig. 5(*a*) resulting in the following two vector equations:

$$\overrightarrow{OM_1} + \overrightarrow{M_1C_1} + \overrightarrow{C_1C_{N/2}} + \overrightarrow{C_{N/2}M_{N/2}} + \overrightarrow{M_{N/2}O} = 0$$
$$\overrightarrow{OM_1} + \overrightarrow{M_1C_1} + \overrightarrow{C_1C_N} + \overrightarrow{C_NM_N} + \overrightarrow{M_NO} = 0 \qquad (13)$$

By decomposing the vector equations into two orthogonal scalar equations along $\vec{x}$ and $\vec{y}$, one can obtain

$$\begin{cases} l_5\cos\theta_O(\cos\beta_2-1)-l_5\sin\theta_O\sin\beta_2 \\ \quad +l_6\cos\theta_M(\cos\alpha_2-1)-l_6\sin\theta_M\sin\alpha_2=p_2\cos\delta_2 \\ l_5\sin\theta_O(\cos\beta_2-1)-l_5\cos\theta_O\sin\beta_2 \\ \quad +l_6\sin\theta_M(\cos\alpha_2-1)-l_6\cos\theta_M\sin\alpha_2=p_2\sin\delta_2 \end{cases} \tag{14}$$

$$\begin{cases} l_5\cos\theta_O(\cos\beta_3-1)-l_5\sin\theta_O\sin\beta_3 \\ \quad +l_6\cos\theta_M(\cos\alpha_3-1)-l_6\sin\theta_M\sin\alpha_3=p_3\cos\delta_3 \\ l_5\sin\theta_O(\cos\beta_3-1)-l_5\cos\theta_O\sin\beta_3 \\ \quad +l_6\sin\theta_M(\cos\alpha_3-1)-l_6\cos\theta_M\sin\alpha_3=p_3\sin\delta_3 \end{cases} \tag{15}$$

The system of equations contains 12 unknowns for four equations. The four variables related to point C, that is p_2, δ_2, p_3, and δ_3, are defined by the generated path obtained from the optimized FBLM-2 model. Moreover, according to constraint #5, link l_6 should rotate Φ_{hinge} between the initial and final positions resulting in $\Phi_{hinge}/2$ between the initial and the intermediate position $N/2$; so that α_2 and α_3 are determined by

$$\begin{cases} \alpha_2=\Phi_{hinge}/2=-16\,\text{deg} \\ \alpha_3=\Phi_{hinge}=-32\,\text{deg} \end{cases} \tag{16}$$

Furthermore, β_2 and β_3 are chosen arbitrarily. The system of equations (14) and (15) can be presented in a matrix form by

$$\begin{bmatrix} A & -B & C & -D \\ F & -G & H & -K \\ B & A & D & C \\ G & F & K & H \end{bmatrix} \begin{Bmatrix} l_{5x} \\ l_{5y} \\ l_{6x} \\ l_{6y} \end{Bmatrix} = \begin{Bmatrix} E \\ L \\ M \\ N \end{Bmatrix} \tag{17}$$

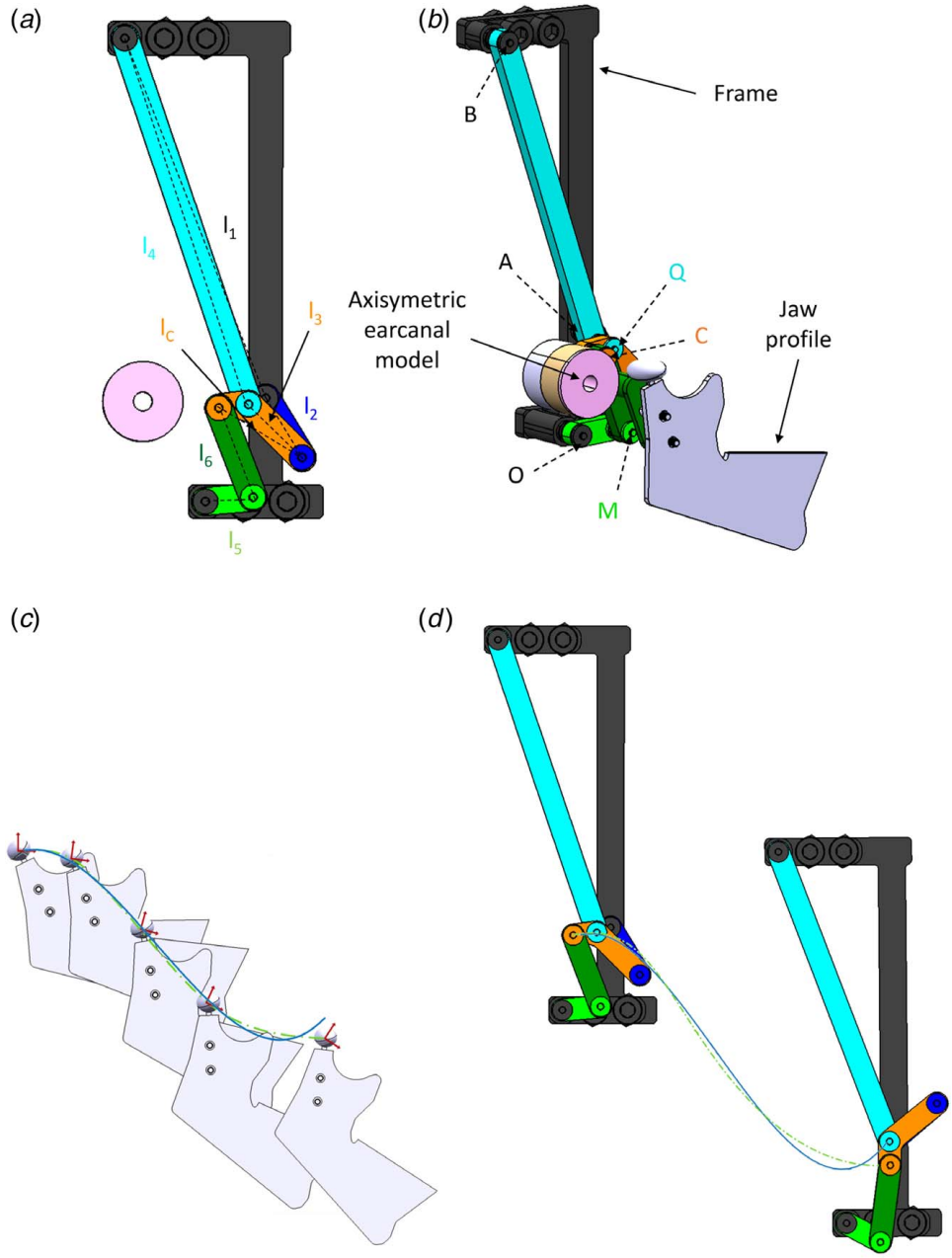

Fig. 7 Computer simulation of the optimized SBLM: (*a*) planar view, (*b*) 3D view with the jaw profile and axisymmetric model of the earcanal, (c) large-scale view of the optimized (dashed-dotted line) and target (solid line) path with the orientation of the jaw along the path, and (*d*) configuration of the mechanism at two extreme positions with the optimized and target path

in which

$$\begin{array}{lll} l_{5x} = l_5 \cos\theta_O & A = \cos\beta_2 - 1 & G = \sin\beta_3 \\ l_{5y} = l_5 \sin\theta_O & B = \sin\beta_2 & H = \cos\alpha_3 - 1 \\ l_{6x} = l_6 \cos\theta_M & C = \cos\alpha_2 - 1 & K = \sin\alpha_3 \\ l_{6y} = l_6 \sin\theta_M & D = \sin\alpha_2 & L = p_3 \cos\delta_3 \\ & E = p_2 \cos\delta_2 & M = p_2 \sin\delta_2 \\ & F = \cos\beta_3 - 1 & N = p_3 \sin\delta_3 \end{array}$$

The solution of the matrix equation gives the link size variables l_{5x}, l_{5y}, l_{6x}, and l_{6y}. By knowing the position of point C, one can find the position of the fixed pivot O by

$$\begin{cases} x_O = x_{C_1} - l_{6x} - l_{5x} \\ y_O = y_{C_1} - l_{6y} - l_{5y} \end{cases} \tag{18}$$

Finally, the analytically synthesized RRR-dyad sub-mechanism can be integrated to the optimized FBLM-2 model to form the six-bar mechanism SBLM capable of generating both the path and the motion of the jaw link during its travel from a closed to open jaw position. The process of the two-phase hybrid approach is outlined in Fig. 6.

5 Results

A two-phase hybrid optimization approach is executed for ten different starting points in both configurations just as for the one-phase approach. The lowest obtained RMSE for the converged solution is calculated to be $\epsilon = 1.29\%$ for the open configuration, with the optimized set of design variables being detailed in Table 2. Moreover, the first-order optimality value is equal to 0.015, which demonstrates a significant improvement over the results that were obtained using the classical one-phase optimization. In addition, the maximum constraint violation value is as low as 4.12×10^{-5}, which guarantees that all the imposed constraints have been satisfied.

The RRR-dyad analytical synthesis for the jaw link's motion generation depends highly on the arbitrary values of β_2 and β_3. Therefore, several couple values of (β_2, β_3) are tested for the RRR-dyad and the obtained feasible designs are marked. Among the marked designs, several candidates are chosen based on the magnitude of the length and rotation of the links to minimize the work space of the mechanism. Finally, the best design is chosen by evaluating the key characteristic criterion of the jaw link rotation, which is the smooth and uniform transition between the initial closed and the final open jaw positions. The values of the chosen angles are $\beta_2 = -25$ deg and $\beta_3 = -35$ deg and the associated values of the design variables are listed in Table 3.

The optimized design of FBLM-2 and analytical synthesis of RRR-dyad are subsequently joined at point C to form the SBLM model. Finally, the computer simulation of the optimally synthesized SBLM shown in Figs. 7(*a*) and 7(*b*) is provided using the computer-assisted design software CATIA V5 (Dassault Systèmes, Vélizy-Villacoublay, France). This virtual prototype enables the verification of the mechanism's global kinematics and validation of the effectiveness of the proposed hybrid approach to replicate the motion of the jaw, as shown in Fig. 7(*c*).

6 Discussion

According to Table 2, the length of all the links is less than 150 mm, as required by constraint #1, the Grashof condition is satisfied as per constraint #2, and l_2 is the shortest link, which meets constraint #3. Therefore, the overall size of the mechanism remains within an acceptable range. The optimized generated path of FBLM-2 (dashed-dotted line) is illustrated in Fig. 8, which also compares it to FBLM-1 (dashed line) and the target path (solid line).

According to Fig. 8, the overall shape of the FBLM-2 curve is much closer to the target path than that of FBLM-1. Particularly, an inflection point and S-shape form can be explicitly observed for the FBLM-2 curve in contrast to FBLM-1's path. Furthermore, the path generated by FBLM-2 is more successful in pursuing the target path, specifically at both extremities of the curves. Since most of the interactions between the earcanal and the TMJ occur at the end of the curve, the accuracy of the generated path at this location is very crucial. The overall improvement achieved by the proposed two-phase hybrid optimization over the classical single-phase optimization can be quantified by comparing their associated errors, which reveals a two-fold increase in performance by the FBLM-2 model. The main reason for this is that the combined path and motion generation synthesis is overconstrained for the FBLM-1 model, whereas the FBLM-2 model is under more reasonable constraints, having had the motion generation constraint assigned to the RRR-dyad sub-mechanism. Therefore, the maximum constraint violation value drops remarkably and becomes almost zero for the path generation synthesis of FBLM-2.

The rotation of jaw link l_6 in the RRR-dyad is calculated while the TMJ is traveling along the trajectory curve. The results for this, demonstrated in Fig. 9, show that the angular variation of the jaw link is almost linear with a constant rate of 2/mm of the TMJ's displacement. From an anatomic point of view, this means

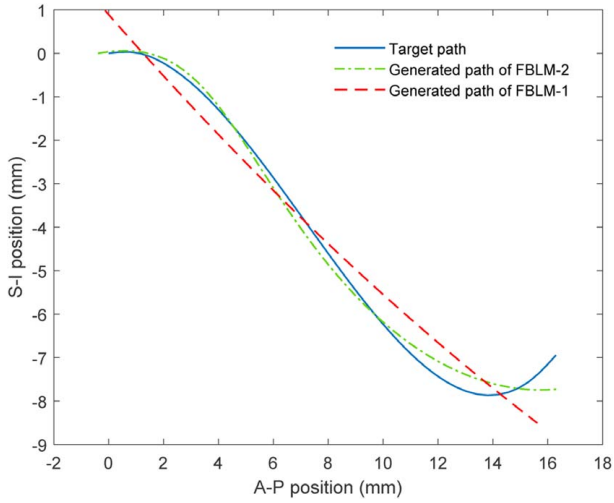

Fig. 8 Optimized generated path for the FBLM-2 model compared with the FBLM-1 and the target path. Closed jaw position corresponds to the origin of the coordinate system.

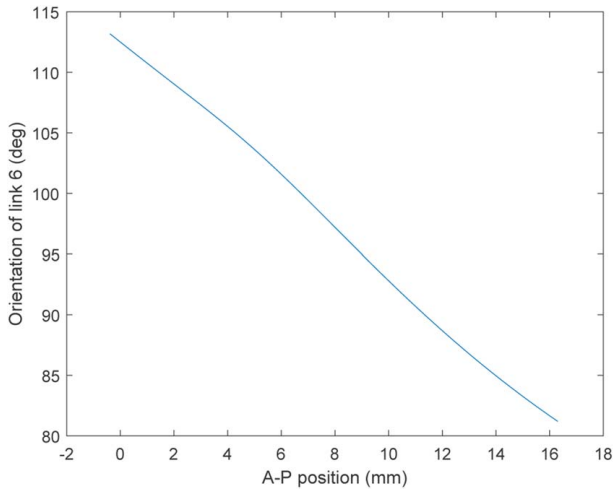

Fig. 9 Angular orientation of the jaw link l_6 according to the A-P position

that the jaw link rotation and translation are mainly done simultaneously which is an integral part of the natural jaw opening and closing cycle. The translation–rotation correlation of the jaw has already been investigated by other researchers. For example, the contribution of the jaw rotation is estimated to be 2.1 ± 0.2 deg/mm of the TMJ's translation [10] showing a difference of about 4.8% compared to what our results report in this research. The difference can be explained by (1) the difference in measuring the horizontal translation of the TMJ (15.0 ± 1.6 mm versus 16 mm used in this work) and (2) the jaw opening rotation around the hinge axis (31.9 ± 4.2 deg versus 32 deg in this work).

As both optimization approaches depend on the initial guesswork used to establish the design variables, the validity of the optimized designs is limited to the vicinity of the initial conjectures. To determine the overall optimal solutions, all the possibilities of the initial speculations would need to be verified.

It should be noted that the human body's anatomy is not unique and hence, the kinematic parameters used to describe the mouth-opening movement may vary among individuals. Three well-individualized kinematic TMJ models correlated with temporal bone geometries have been reported in the literature and it is estimated that the inter-individual variation of the parameters is weak within each group [10]. All the results obtained in this study are closely dependent on the TMJ model described in Sec. 2.

However, the proposed synthesis approach could make it possible to customize the SBLM generated path to model more than one TMJ anatomy. The solving process detailed in Fig. 6 would remain the same, and only the biomechanical constraint values would be adjusted according to the TMJ anatomical model. In addition, the prototype could integrate threaded rods, adjustment spacers, and a compass-like coupler. This design could make it possible to adjust all the link lengths and the coupler angle in order to take into account the variability of the TMJ's anatomy.

7 Conclusions

This paper presents a two-phase motion generation synthesis which enables designing a six-bar kinematic simulator consisting of a four-bar mechanism and RRR-dyad linkage. The complexity of the objective function to minimize the error between the anatomical target path and the mechanism's generated curve as well as the strong nonlinear constraints imposed by the anatomy of the jaw movements rendered the solution consisting of a simple FBLM-1 insufficient. Accordingly, the associated design became overconstrained and the classical single-phase optimization approach could not return an acceptable converged solution. Therefore, the two-phase optimization approach was proposed, splitting the path and motion generation of the jaw movement between two different sub-mechanisms. Subsequently, the solution of a nonlinear optimization involving a properly constrained FBLM-2 was integrated into an analytical solution for the three-position synthesis of a two-link dyad (RRR-dyad).

The results prove the effectiveness of the proposed synthesis approach in reproducing the TMJ path as well as replicating the jaw rotation during a typical jaw opening motion. In addition, the required correlation between the translation of the TMJ and the rotation of the jaw could be successfully achieved by the optimized mechanism assuring that the generated movement is close to the natural jaw opening motion. The synchronization of movements has not been sought in this paper, however the synthesized mechanism would be capable of generating the synchronous movement with the natural movement of the jaw through an appropriate control of the input crank angle.

The proposed two-phase optimization approach can be further used to design linkage mechanisms in general and human prosthesis in particular where complicated objective functions and highly nonlinear constraints impair the use of the classical optimization approach. Moreover, the developed kinematic simulator would facilitate the morphological study of the TMJ and the deformation analysis of the earcanal while providing a platform to validate the kinematic mechanisms, biomechanical computer simulations, or finite element models of the TMJ–earcanal interactions. Additionally, the proposed simulator can give new insights into the complex motion of the TMJ, improve mandibular implant design, and eventually lead to a better understanding and treatment of TMJ diseases. Furthermore, this approach can enable the investigation of discomfort issues related to hearing prostheses and simplify the evaluation of the kinetic energy associated with earcanal dynamic movements for energy harvesting.

Acknowledgment

The authors would like to acknowledge the support of the Natural Sciences and Engineering Council of Canada (NSERC), through the last author's Discovery grant (RGPIN-2017-06192). The technical support received from the NSERC-EERS Industrial Research Chair in In-Ear Technologies (CRITIAS) is also greatly appreciated.

Conflict of Interest

There are no conflicts of interest.

Data Availability Statement

The authors attest that all data for this study are included in the paper.

References

[1] Delnavaz, A., and Voix, J., 2013, "Ear Canal Dynamic Motion as a Source of Power for In-Ear Devices," J. Appl. Phys., **113**(6), p. 064701.

[2] Bouchard-Roy, J., Delnavaz, A., and Voix, J., 2020, "In-Ear Energy Harvesting: Evaluation of the Power Capability of the Temporomandibular Joint," IEEE Sens. J., **20**(12), pp. 6338–6345.

[3] Carioli, J., Delnavaz, A., Zednik, R. J., and Voix, J., 2016, "Power Capacity From Earcanal Dynamic Motion," AIP Adv., **6**(12), p. 125203.

[4] Travers, K. H., Buschang, P. H., Hayasaki, H., and Throckmorton, G. S., 2000, "Associations Between Incisor and Mandibular Condylar Movements During Maximum Mouth Opening in Humans," Arch. Oral Biol., **45**(4), pp. 267–275.

[5] Koolstra, J., Naeije, M., and Van Eijden, T., 2001, "The Three-Dimensional Active Envelope of Jaw Border Movement and Its Determinants," J. Dent. Res., **80**(10), pp. 1908–1912.

[6] Azuma, T., Ito, J., Kutsuki, M., Nakai, R., Fujita, S., and Tsutsumi, S., 2009, "Analysis of the Mandibular Movement by Simultaneous Multisection Continuous Ultrafast MRI," Magn. Reson. Imag., **27**(3), pp. 423–433.

[7] Baeyens, J.-P., Gilomen, H., Erdmann, B., Clijsen, R., Cabri, J., and Vissers, D., 2013, "In Vivo Measurement of the 3D Kinematics of the Temporomandibular Joint Using Miniaturized Electromagnetic Trackers: Technical Report," Med. Biol. Eng. Comput., **51**(4), pp. 479–484.

[8] Yatabe, M., Zwijnenburg, A., Megens, C., and Naeije, M., 1997, "Movements of the Mandibular Condyle Kinematic Center During Jaw Opening and Closing," J. Dent. Res., **76**(2), pp. 714–719.

[9] Ahn, S.-J., Tsou, L., Antonio Sánchez, C., Fels, S., and Kwon, H.-B., 2015, "Analyzing Center of Rotation During Opening and Closing Movements of the Mandible Using Computer Simulations," J. Biomech., **48**(4), pp. 666–671.

[10] Mesnard, M., Coutant, J. C., Aoun, M., Morlier, J., Cid, M., and Caix, P., 2012, "Relationships Between Geometry and Kinematic Characteristics in the Temporomandibular Joint," Comput. Methods Biomech. Biomed. Eng., **15**(4), pp. 393–400.

[11] Chen, C.-C., Lin, C.-C., Lu, T.-W., Chiang, H., and Chen, Y.-J., 2013, "Feasibility of Differential Quantification of 3D Temporomandibular Kinematics During Various Oral Activities Using a Cone-Beam Computed Tomography-Based 3D Fluoroscopic Method," J. Dent. Sci., **8**(2), pp. 151–159.

[12] Gallo, L., Airoldi, G., Airoldi, R., and Palla, S., 1997, "Description of Mandibular Finite Helical Axis Pathways in Asymptomatic Subjects," J. Dent. Res., **76**(2), pp. 704–713.

[13] Hayashi, K., Hayashi, M., Reich, B., Lee, S.-P., Sachdeva, A. U. C., and Mizoguchi, I., 2012, "Functional Data Analysis of Mandibular Movement Using Third-Degree B-Spline Basis Functions and Self-Modeling Regression," Orthod. Waves, **71**(1), pp. 17–25.

[14] Takanobu, H., Takanishi, A., and Kato, I., 1994, "Control of a Mastication Robot for Reduction of Jaw Joint Force Focusing on Musculus Temporalis," Proceedings of IEEE/RSJ International Conference on Intelligent Robots and Systems (IROS'94), Munich, Germany, Sept. 12–16, Vol. 3, IEEE, pp. 1824–1831.

[15] Takanishi, A., Tanase, T., Kumei, M., and Kato, I., 1991, "Development of 3 DOF Jaw Robot WJ-2 as a Human's Mastication Simulator," Fifth International Conference on Advanced Robotics' Robots in Unstructured Environments, Pisa, Italy, June 19–22, Vol. 1, IEEE, pp. 277–282.
[16] Takanobu, H., Yajima, T., Nakazawa, M., Takanishi, A., Ohtsuki, K., and Ohnishi, M., 1998, "Quantification of Masticatory Efficiency With a Mastication Robot," Proceedings 1998 IEEE International Conference on Robotics and Automation (Cat. No. 98CH36146), Leuven, Belgium, May 16–21, Vol. 2, IEEE, pp. 1635–1640.
[17] Galer, B., Hockenberry, N., Maloof, J., and Monte-Lowry, M., 2007, "Human Jaw Motion Simulator," Technical Design Paper 65, April, Northeaster University, Boston, MA.
[18] Tahir, A. M., Jilich, M., Trinh, D. C., Cannata, G., Barberis, F., and Zoppi, M., 2019, "Architecture and Design of a Robotic Mastication Simulator for Interactive Load Testing of Dental Implants and the Mandible," J. Prosthet. Dent., **122**(4), pp. 389.e1–389.e8.
[19] Mostashiri, N., Dhupia, J., Verl, A., Bronlund, J., and Xu, W., 2020, "Optimizing the Torque Distribution of a Redundantly Actuated Parallel Robot to Study the Temporomandibular Reaction Forces During Food Chewing," ASME J. Mech. Rob., **12**(5), p. 051008.
[20] Pirzanski, C., and Berge, B., 2005, "Ear Canal Dynamics: Facts Versus Perception," Hear. J., **58**(10), p. 50.
[21] Pirzanski, C., 2010, "Earmold Retention Issues: Why Does This Earmold Keep Falling Out?," Hear. Rev., **17**(5), pp. 26–34.
[22] Nielsen, C., and Darkner, S., 2011, "The Cartilage Bone Junction and Its Implication for Deep Canal Hearing Instrument Fittings," Hear. J., **64**(3), p. 35.
[23] Haulin, E. N., Lakis, A. A., and Vinet, R., 2001, "Optimal Synthesis of a Planar Four-Link Mechanism Used in a Hand Prosthesis," Mech. Mach. Theory, **36**(11), pp. 1203–1214.
[24] Tsuge, B. Y., Plecnik, M. M., and Michael McCarthy, J., 2016, "Homotopy Directed Optimization to Design a Six-Bar Linkage for a Lower Limb With a Natural Ankle Trajectory," ASME J. Mech. Rob., **8**(6), p. 061009.
[25] Guo, G., Zhang, J., and Gruver, W. A., 1993, "Optimal Design of a Six-Bar Linkage With One Degree of Freedom for an Anthropomorphic Three-Jointed Finger Mechanism," Proc. Inst. Mech. Eng. Part H: J. Eng. Med., **207**(3), pp. 185–190.
[26] Doutres, O., Sgard, F., Terroir, J., Perrin, N., Jolly, C., Gauvin, C., and Negrini, A., 2019, "A Critical Review of the Literature on Comfort of Hearing Protection Devices: Definition of Comfort and Identification of Its Main Attributes for Earplug Types," Int. J. Audiol., **58**(12), pp. 824–833.
[27] Kochkin, S., 2000, "MarkeTrak V: "Why My Hearing Aids are in the Drawer," Hear. J., **53**(2), p. 34.
[28] Berger, E. H., and Voix, J., 2018, *The Noise Manual*, 6th ed., D. K. Meinke, E. H. Berger, R. Neitzel, D. P. Driscoll, and L. D. Hager, eds., American Industrial Hygiene Association, Falls Church, VA, pp. 379–454.
[29] Delnavaz, A., and Voix, J., 2014, "Energy Harvesting for In-Ear Devices Using Ear Canal Dynamic Motion," IEEE Trans. Ind. Electron., **61**(1), pp. 583–590.
[30] Delnavaz, A., and Voix, J., 2014, "Flexible Piezoelectric Energy Harvesting From Jaw Movements," Smart Mater. Struct., **23**(10), p. 105020.
[31] Carioli, J., Delnavaz, A., Zednik, R. J., and Voix, J., 2018, "Piezoelectric Earcanal Bending Sensor," IEEE Sens. J., **18**(5), pp. 2060–2067.
[32] Peck, C. C., Langenbach, G. E. J., and Hannam, A. G., 2000, "Dynamic Simulation of Muscle and Articular Properties During Human Wide Jaw Opening," Arch. Oral Biol., **45**(11), pp. 963–982.
[33] Simón Mata, A., Bataller Torras, A., Cabrera Carrillo, J. A., Ezquerro Juanco, F., Guerra Fernández, A. J., Nadal Martínez, F., and Ortiz Fernández, A., 2016, *Fundamentals of Machine Theory and Mechanisms*, 1, Vol. 40, Springer International Publishing, Cham, pp. 1–409.